HArtMuT - Modeling eye and muscle contributors in neuroelectric imaging

Nils Harmening[1], Marius Klug[2], Klaus Gramann[2], and Daniel Miklody[1]

[1]Technische Universität Berlin, Neurotechnology
[2]Technische Universität Berlin, Biological Psychology and Neuroergonomics

March 29, 2022

Abstract

Electroencephalography (EEG) and Magnetoencephalograhy (MEG) data are mostly mixed with activity stemming from the eyes and muscles. Neuroscientific researchers decrease the effect of these non-brain sources on the recorded data using artefact cleaning methods operating in sensor space (e.g. filtering, subtracting signals from additional eye or neck electrodes) or by removal of automatically or manually identified independent or principal components (ICs/PCs). The subsequent source localization techniques are commonly applied to data that was cleaned from such physiological sources and other non-physiological artefacts. However, this chronological procedure leads to distorted EEG time series due to imperfect artefact reduction routines, introduces a bias into the subsequent source localization and excludes potentially interesting additional information.
Therefore, we propose adding sources that are usually considered artefactual to the head model in a similar way as it is done for cortical sources. Treating muscles and eyes as proper contributors to EEG potentials allows for a more precise identification of these sources that can then be ignored or excluded automatically for further data analyses.

We developed a head artefact model using tripoles (HArtMuT) - a volume conduction head model with cortical dipole sources enhanced by symmetric dipoles for the eyes and tripoles for face and neck muscles. HArtMuT can be used for modeling eye and muscle contributors to the EEG signal, cortical and artefactual source reconstruction and for evaluating or constructing algorithms.

We compared different artefact modelling approaches using physiologically motivated dipolar and tripolar source models. Their performance was evaluated with respect to source localization accuracy using as ground truth both simulated HD-FEM data and ICA patterns from EEG recordings of 19 subjects completing different body rotation tasks.

The best model for neural sources were found to be the standard equivalent dipole, while the eyes were better approximated by symmetric dipolar models. The muscular contributors were also well in accordance with a dipolar model but a better approximation of source location was achieved with tripoles. Preliminary results show a possible usage as classifiers of the resulting source locations for identifying neural and artefactual sources. Compared to using standard EEGLAB 3-shell models on real ICA-decomposed data, the residual variance was reduced from median 0.25 to 0.11 for muscle sources and 0.18 to 0.09 for eye sources. 68% of the ICA patterns were detected as muscle sources based on source location in the 4-shell HArtMuT, while 30% were brain and around 2% symmetric eye sources.

Introduction

Magenetoencephalography (MEG) and Electroencephalography (EEG) are methods to non-invasively measure the electrical activity of neurons in humans and other species. EEG provides high temporal but only limited spatial resolution, because of the sensors being placed on the scalp outside the low-conductive skull. Due to volume conduction, only a spatially smeared linear mixture of all cortical sources, that are active in parallel, arrives at the sensor level [Haufe et al., 2014]. MEG has better spatial resolution than EEG, since the magnetic fields are less distorted by the mixture of different conductive tissues (brain, cerebro-spinal fluid (CSF), skull, skin), but suffers from low signal-to-noise ratio in particular for deeper sources. In addition, MEG is sensitive primarily to tangential oriented sources and is more demanding in its recording procedure.

Both MEG and EEG, referred to as M/EEG in the following, record volume conducted signals composed of cortical sources active in parallel and mixing in a linear fashion. Dissociating the different sources can be solved based on source separation techniques [Pearson, 1901, Makeig et al., 1996a, Blankertz et al., 2011], introducing a number of assumption to solve the ill-posed inverse problem [Sarvas, 1987]. Mathematically dissociating cortical sources in the M/EEG signal is further complicated by other sources contributing to the recorded signal, like physiological non-brain sources (eye movement, muscle activity) and mechanical (cable sway in EEG) or electrical sources (noise stemming from stimulation monitors and other devices).

While mechanical sources often show invariant patterns, that can be easily dissociated, eye movement and muscle activity of facial and neck muscles are often less easy to identify. Importantly, these classes of non-brain sources contribute significantly to the signal as they are located outside the skull and show higher energy compared to the minuscule EEG signal. Signals from eye movements and blinks can be orders of magnitude larger than brain-generated electrical potential and activity stemming from eye movements, the closure of the lid and its necessary muscular activity and neck and face muscle activity are the most common types of artefacts in EEG recordings .

This kind of non-brain activity is traditionally considered to be artefactual, even though eye movement and facial mimicry significantly contribute to or are a result of cognitive and affective processes (REF). As a consequence, a number of artefact rejection methods has evolved to identify and remove such kind of activity from the recorded signal. Rejecting contaminated trials, however, causes substantial data loss, and restricting eye movements/blinks might limit the experimental design and could impact the cognitive processes under investigation. Thus, newer algorithms attempt to remove artefact specific features from the signal without deleting contaminated time periods to preserve as much data as possible .

Among these algorithms are blind source separation (BSS) techniques [Urigüen and Zapirain, 2015] that decompose the signal mostly based on its spatio-temporal statistics into different sources after which neural sources are identified and separated. The most commonly used approach is Independent Component Analysis (ICA) which separates the sources based on the principle of maximal statistical independence. The assumption that neural and artefactual sources are independent implies the possibility of sorting them into sources of different origin. This can be done manually by an expert or automatic routines can be applied [Winkler et al., 2011, Pion-Tonachini et al., 2019].

Eventually, the sources that have been identified as originating in the brain, are further localized using source localization approaches . Locating the sources in general requires a forward solution which contains the location generating the activity. The same approaches could be used to localize other physiological sources, however, to our knowledge no head model actually provides leadfields that incorporate the eyes and facial as well as neck muscles in the forward solution.

On the other hand, the simulation of different signal sources including those of eyes and muscles is useful for educational and validational purposes, like it has been done for neural origins [Krol et al., 2018]. This also involves the modeling of a biophysical forward model, that mimics the field propagation within the head and is so far done almost exclusively for neural sources in existing models.

In order to improve the source localization accuracy, to provide a better guide for users to distinguish brain from non-brain sources and to provide a model, which is suitable for eye and muscle simulations, we propose our Head Artefact Model using Tripoles (HArtMuT). Calculated with Boundary and Finite Element Methods (BEM/FEM) for different commonly used standard head anatomies, the model incorporates eyes, facial muscles and muscles in the dorsal neck region into EEG leadfields and is ready to be implemented into standard approaches of all kind.

The aim of this study was to use an artefact source model as extension to the existing cortical source model for solving the inverse problem and improving localization of non-brain sources that contribute to M/EEG recordings. Therefore, we developed the so called HArtMuT, a 4-shell Boundary Element Method (BEM) head model [Gramfort et al., 2010] of the anatomy of Colin [Holmes et al., 1998], consisting of a cortex (gray + white matter), cerebrospinal fluid (CSF), skull and neck extended scalp mesh. The model

was segmented using an automatic segmentation pipeline with final surface mesh sizes of 1922 vertices and 3990 triangles each. This has proven to be a reasonable compromise between model size, hence accuracy, and computational speed during inverse fit methods with inverse nonlinear fit requiring frequent leadfield recalculation [Miklody et al., 2016, Miklody, 2020].

Source modelling

While EEG artefacts of instrumental original can be diminished by thorough experimental setup designs, artefacts of physiologic origin cannot be avoided a priori and are part of the measurement. Commonly, only neuronal sources are simulated in head models, leading to erroneous localization of muscular or ocular sources within the brain. The motivation of this study was therefore to represent all EEG signal contributors of biological origin adequately in the modeling process. This allows to better model non-brain physiological activity and to use such activity for later analyses as it might be significantly linked to the cognitive processes of interest. This approach further enables a better classification of brain and non-brain sources as the latter are not incorrectly localized into the brain anymore. We investigated cortical, ocular, and muscular artefacts by using electric field models derived from their activity. In the lower frequencies ($< 1\,\mathrm{kHz}$), the basis of common electrical models of volume conduction in the human head is the quasi-electrostatic assumption [Häamäläinen et al., 1993] which leads to a Poisson equation that has to be solved in order to model the field distributions (see e.g. Sarvas [1987]):

$$\nabla \cdot (\sigma \nabla \Phi)) = \nabla \cdot \vec{J_P} \tag{1}$$

$\vec{J_P}$ are the sources of primary currents, that lead to the volume conduction $\vec{J} = \sigma \nabla \Phi$. $\vec{J_P}$ are usually modeled as a superposition of point sources like single dipoles called the equivalent current dipole (ECD). The sources produce a local current flow which leads to a return current in all connected conductive tissue. The infinite homogeneous solutions of eqn. 1 for a given geometry with the ECD as J_P are commonly used to simulate the electrical potential of a firing population of neurons. These solutions are unique and can be numerically determined. The most common numerical methods nowadays are Boundary Element Method (BEM), Finite Element Method (FEM) and Finite Differences Method (FDM). In general, FEM/FDMs can incorporate more detail in anatomy and conductivity, such as anistropy or certain local inhomogeneities, but are computationally much more expensive.

We will now look into the physiology of the different source types, the resulting fields and models.

Cortical sources

The main neuronal activity is believed to be based on membrane potentials and electrical currents through ions. Whether being Action Potentials (AP) along the Axons or Postsynaptic Potentials (PSP), they produce a current flow through the membrane, that leads to a secondary return current flow through the neuron's surrounding, which can be measured outside the head [Buzsáki et al., 2012]. In particular scalp EEG is assumed to be primarily elicited by the mean field produced by PSPs of neocortex layer pyramidal cells in the cerebrum. The ECD is a widely accepted approximation for the electric field of a population of parallel aligned and synchronously firing neurons. For a detailed derivation of the ECD from the contribution of principal neocortical neurons to the EEG, please refer to Murakami and Okada [2006].

The far-field of an ECD is described by an analytic expression, which is then used in combination with the headmodel to describe the resulting volume conduction within the whole head. In Cartesian coordinates, this electrical far-field potential of a dipolar current source in an infinite homogeneous conductive medium is

$$\phi_d(\vec{r}, \vec{r}_q) = \frac{1}{4\pi\sigma} \frac{\vec{Q} \cdot (\vec{r} - \vec{r}_q)}{|\vec{r} - \vec{r}_q|^3} \quad . \tag{2}$$

And the current density is calculated as

$$\vec{J}_d(\vec{r},\vec{r}_q) = \frac{1}{4\pi}\left(3\frac{(\vec{r}-\vec{r}_q)\cdot\vec{Q}}{|\vec{r}-\vec{r}_q|^5}\cdot(\vec{r}-\vec{r}_q) - \frac{\vec{Q}}{|\vec{r}-\vec{r}_q|^3}\right) \quad , \tag{3}$$

where σ is the specific conductivity of the material and $\vec{Q}$ is the local current density produced by the source. $\vec{r}$ is the observed point and the position of the source is $\vec{r}_q$. We will later use the fact, that the far-field can be seen as an approximation based on two monopoles with distance $\vec{d}$ and $\vec{Q} = q * \vec{d}$, where terms of order $O\left[\left(|\vec{d}|/|\vec{r}|\right)^2\right]$ are omitted, because it is assumed that $|\vec{r}| \gg \left|\vec{d}\right|$.

Ocular sources

Ocular artefacts in the EEG are caused by eye movements or blinks and are associated with higher amplitudes and lower frequencies than those of cortical EEG signals. The underlying sources are mainly charge distributions in the eyeball, but additionally include the eye muscles, that produce an electrical field when active and the closure of the eyelids, that modifies the volume conduction. The eyes are mostly the components of strongest amplitude and can be easily identified by their specific frontal patterns. Eye movements of both eyes are generally linked in healthy humans leading to a common resulting field produced by both eyes equally. Since the potentials are correlated among both eyes, single eye sources cannot be separated by ICA/PCA. This symmetry therefore has to be incorporated into the model, which is tested by investigating single and symmetric eye models.

Physiology

The eyes are electrically charged at different structures as depicted in fig. 1. Firstly, the photoreceptors in the retina maintain a standing negative resting potential in order to turn incoming light into an excitation. In the pigment epithelium this results in an electrical signal, which then propagates through the optic nerve to the visual cortex. Contrary to this strong negative charge distribution, fewer positive potassium and sodium ions are located in the outer segment of the photoreceptor cells, forming the overall membrane potential of around $-40\,\mathrm{mV}$. When stimulated, the photoreceptors become even more hyperpolarized. Opposing the retinas negativity is the overall positivity of the cornea. In its function to protect the frontal eye from physical and chemical agents, it transports positively charged sodium ions inward and negatively charged chloride ions outward, such that its surface, the corneal epithelium, is again negatively charged. During eye movements or blinks, the described charge distributions move and their electrical field changes. Since it is these changes, that are recorded as EOG, an equivalent ocular model is expected to describe the charge distribution difference pre and post movement rather than the static charge distributions. Additionally, the eyeball rotation is driven by small muscles around the eyes, that produce an electrical field when active, which should be included into the muscle model. The closure of the eyelid is thought to additionally change the local field by altering the geometry of the volume conductor [Plöchl et al., 2012]. A model for this is out of scope of this paper.

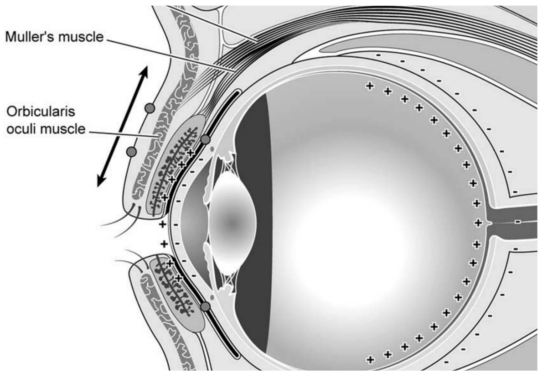

Figure 1: Anatomy and charge distribution of the eye and eyelid. In the right, the negatively charged (−) retina and its opposing smaller positive charges (+), and in the left, the inside positivity of the cornea and its surface negativity. An eyeball rotation results in charge distribution differences, that are visible in the EEG. The eyelid itself consists of the Orbicularis oculi muscle and its sliding is functioned by Muller's muscle. The eyeball rotation muscles are omitted in this schematic depiction for the sake of simplicity. Reprinted from Iwasaki et al. [2005], Copyright 2004, with permission from Elsevier.

Literature overview
Some studies already investigated modeling the contribution of eye activity to EEG signals, where the strong corneo-retinal potential was mostly approximated by one equivalent ocular dipole with its negative pole posteriorly (directed towards the retina) and its positive pole anteriorly (directed towards the cornea). Using EOG recorded signals during vertical and horizontal eye movements and eye blinks, Berg and Scherg [1991] observed, that '*a reasonable fit was only obtained if the equivalent dipoles were allowed to take up different locations and orientations depending on the type of eye activity*'. A single dipole was determined for each movement across subjects. However, the difference dipole of a single eye movement was assumed to be approximately stationary due to asking the subjects to move their eyes always by the same fixed angle. Therefore, one might conjecture, that even more equivalent dipoles for the same movement direction but different angles are needed. One specific dipole per eye was also determined to approximate the EOG signal during eye blinks. This dipole bears analogy to that of vertical eye movements, which reflects Bell's phenomenon: '*Spontaneous blinks produced small eye movements directed down and inward, whereas slow or forced blinks were associated with delayed upward eye rotations*', as stated by [Iwasaki et al., 2005]. They undertook a detailed EOG analysis of eye and lid movements, reasoning that '*EOG signals during vertical eye- and lid-movements are greatly influenced by the eyelids*', since a closed eye lid conducts the ocular dipole field to the fronto-polar scalp region within the scalp tissue.

Summary
Most studies investigated the approximation of the large corneoretinal potential by an equivalent dipole. However, in order to mirror the actual biological charge distribution differences correctly, monopolar sources could be placed into the retina and the cornea, respectively, which is technically demanding. In order to approximate the actual charge distributions, the monopoles can be replaced by dipoles. Corresponding to eyeball rotations, activity of the extraocular muscles is expected, as well as muller's muscle activity due to eye lid closures during blinks.
Additionally, we hypothesize, that both eyes move simultaneously and synchronously during regular usage in healthy subjects, which leads to an electric field and therefor patterns stemming from two sources - one in each eye. To this extent, we included symmetric dipolar fields into HArtMuT, that consist of a summation of left and right eye positions with identical orientation vector. The performance of the different ocular models (single and eye-symmetric dipoles together with tripolar sources in the eye muscles) were investigated. The same dipolar model as used for the brain (eq. 2 and 3) and the same tripolar model as used for the muscles (eq. 6 and 7) are obeyed for dipolar and tripolar sources, respectively.

Musclular sources

Muscular activity is usually measured using bipolar electromyography (EMG) recordings. Several muscles are located in the face and on the human skull as well as in the posterior and anterior neck regions. Due to their strong activity patterns because of their location outside the skull, EMG activity is often observed in EEG recordings. In traditional M/EEG protocols participants are restrained in their movements and supracranial and facial muscles contribute to the EEG signal mainly in the higher frequency range starting at around 20 Hz. However, newer mobile EEG and Mobile Brain/Body Imaging studies demonstrated a strong contribution of neck muscles in moving participants with a contribution of lower frequencies in addition to the known higher frequency range from other muscles. Thus, it is even more important to dissociate this non-brain activity from the activity of interest, also in lower frequencies. Most of these muscle artefacts are larger in amplitude than the neuro-electric activity measured at the scalp. Their spatial scalp patterns differ from those of neural origin, since their sources are located directly in the scalp in close proximity to the EEG cap, and their field is thus more local and on the boundaries. Additionally, due to their physiological properties, they have a rather tripolar field distribution, which has certain impacts on the patterns as well.

Physiology
Skeletal muscles are composed of bundles of muscle fibers, that are long cylindrical cells containing many myofibrils composed of contractile units called sarcomeres. The muscle fibers and the corresponding motor

neuron of the nervous system are connected via nerve fibers that divide into many terminal branches. Each chemical synapse of these axon terminals builds a so-called neuromuscular junction, ending on a specific region of the muscle fiber, called the motor end plate. When the nerve impulse for muscle contraction in form of an action potential reaches this neuromuscular junction, synaptic transmission to the muscle fiber begins. The action potential triggers a chemical process which leads to a depolarization of the resting membrane potential of approximately -70 mV. If the threshold potential (often between around -55 and -50 mV) is exceeded, the electrical impuls of the end plate's potential travels down the traverse tubules (T tubules) into the interior of the muscle fiber and finally triggers the contraction of all sarcomeres.
This depolarization and the subsequent re-polarization phase, called hyperpolarization, is followed by the afterhyperpolarization (AHP), in which the membrane potential falls below the resting potential until it returns to its normal resting voltage.
The muscle fibers innervated by a single axon are known as the muscle unit. Those muscle units innervated by the same motor neuron form together with its motor neuron a single motor unit (MU), such that a motor unit action potential (MUAP) is produced by the summation of the accompanying muscle unit's end plate potentials. Upon muscle contraction, the generated MUAPs and their propagation from the muscle end plate to the tendons are recorded during electromyography (EMG) and as unwanted artefacts during EEG. This propagation in several muscle fibers leads to an EMG signal, originating from multiple distributed source locations, and is thus rather a mean field signal.

Literature overview

While modeling ocular contributors to the EEG have already been discussed among researchers, muscular sources - to our knowledge - have not been added to any head model so far.

However, approaches in modelling EMG sources exist in particular for sources in the extremities. Some researchers used a simple dipole to approximate the MUAP's curve [Boyd et al., 1978] [Winter et al., 1994], while others used (two) balanced tripoles pointing opposingly into the direction of the muscle fiber ends [Farina and Rainoldi, 1999], [Griep et al., 1982], [Merletti et al., 1999], [Roeleveld et al., 1997]. The potential curve appears more tripolar with a skewness related to the tripolar asymmetry in propagation direction, when taking into account also the AHP, thus the negative sink after the action potential peak (fig. 2). As shown by Merletti and Farina [2016], the field of an equivalent tripolar source model has a similar curvature to the more realistic analytic waveform, that were originally developed by Rosenfalck [1969] and later modified by Nandedkar and Stålberg [1983].

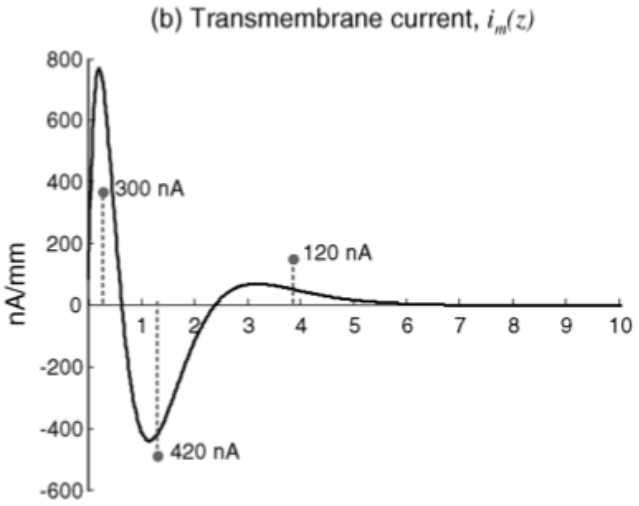

Figure 2: Simulated transmembrane current per unit length (based on Nandedkar and Stålberg [1983]) and the equivalent tripole source model as approximated by Merletti and Farina [2016]. The electric field of the first positive (300 nA) and the negative (420 nA) sources corresponds to the depolarization and the subsequent re-polarization phase. This would be covered by an equivalent dipolar current source model. Adding the second positive charge (120 nA) a bit apart, additionally incorporates the following small AHP bump. This constitutes the equivalent tripolar current source model solution. Fig. reprinted with permission from Merletti and Farina [2016]. Copyright 2016 by The Institute of Electrical and Electronics Engineers, Inc.

Thoughts on MUAPs in human head

In the human head, these muscular sources are found within what is usually modeled as scalp: a thinner sheet of conductive tissue bordering the non-conductive air and the much less conductive skull (estimated conductivity ratio 1:40 to 1:80 [Goncalves et al., 2003, Clerc et al., 2005]). These rather sudden changes of conductivity also have an effect on the inner distributions of electrical potential and current flow. In figure 3 we can observe that depending on the orientation of the tripole relative to the measured surface potential, it can have one, two or three focal patterns on the surface. MUAP models vary in charge distribution and locations of the three monopoles, that form the tripole. Furthermore, the line, on which the three monopoles are places, is not necessarily straight but can also be curved. All this has effects on the appearance as surface potentials.

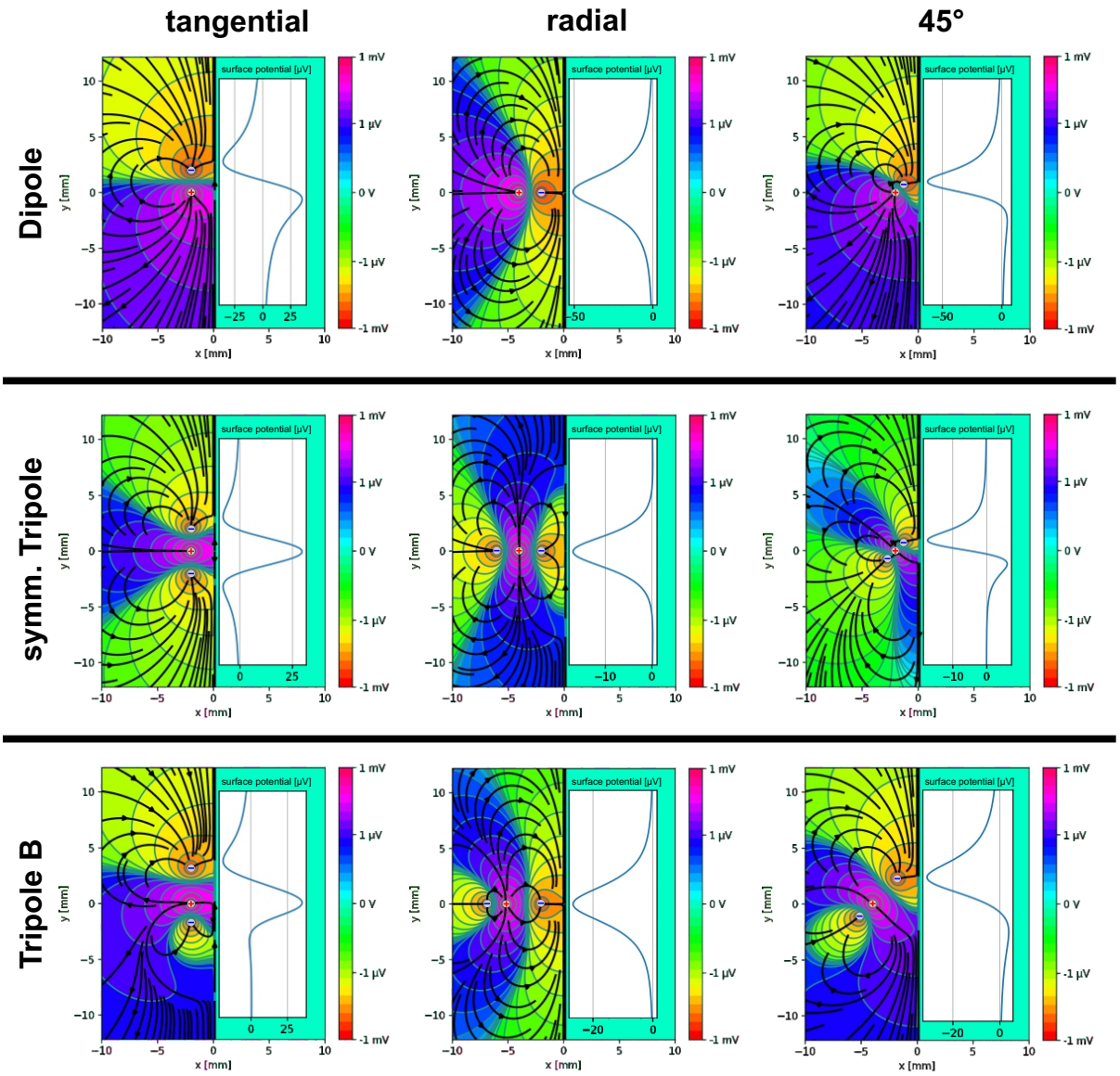

Figure 3: Head model simulations of three different equivalent current tripole orientations (tangential, radial, 45°) at the same source position. Different orientations lead to different surface potentials patterns: A tripole can look similar to a dipole or a monopole depending on its orientation, however certain characteristics like the fall-off with distance differ. The *dipole* (upper row) consists of a double negative sink and a double positive source. The *symmetric tripole* (middle row) consists of two negative sinks the same distance in opposite direction apart from a double positive source. *Tripole B* additionally has different distances leading to a rather dipolar potential distribution. The surface at $x = 0$ is to a non-conductive domain for $x > 0$, which simulates the scalp surface touching air. The lines depict different voltage levels (iso-voltage lines), while the flow lines represent the current flow (the density of the lines is arbitrary).

The central (in our case positive) peaks of tripoles decay faster in amplitude than dipolar peaks, but compared to brain sources, the missing spatial smearing effect of the CSF and skull additionally leads to more focal patterns for scalp sources. If tripoles are modeled similar as in Merletti and Farina [2016] (see fig. 2),

the resulting field is in transition between dipole and tripole as the closer and stronger pair of sources (300nA/420nA) dominates the field, as we can see in figure 3.

Summary
Due to existing evidence for both approaches, dipolar and tripolar, we decided to test both, as they can also be physiologically motivated.
Moreover, little is known about EMG signals fall-off in current flow power within the muscle fibers [Kuiken et al., 2001], that, strictly speaking, one would additionally need to take into account. Since the potential form of EMG signals at different fiber positions is not simply a delayed versions of each other [Merletti and Farina, 2016], we place several myogenic sources along the signal's two propagation directions from the neuromuscular junction (NMJ) to the tendons in the model. For source reconstruction, no restrictions will be set to positions within the scalp in order to avoid systematic modeling errors due to incorrect segmentation or generic head models. Sources are then assigned the label of the closest muscle for identification.
Because the distance between the sources is in a similar range as the distance to the surface, a far field approximation, such as that used for equivalent current dipoles for neurons inside the brain, does not hold for sources outside the skull. Instead, the optimal model would be directly modeling the current flow out of the muscle along its fibers using analytic solutions comparable to Nandedkar and Stålberg [1983]. Such an implementation in existing head model software would not allow the usage of most existing inverse fitting approaches, that optimize location and orientation of point sources. We therefore model the tripolar structure as three single monopolar sources, as described by Merletti and Farina [2016]. In Cartesian coordinates, the electrical field potential of a single (monpolar) current source ϕ_m in an infinite homogeneous conductive medium is calcalted as

$$\phi_m(\vec{r}, \vec{r}_q)) = \frac{I}{4\pi\sigma} \frac{1}{|\vec{r} - \vec{r}_q|} \quad . \tag{4}$$

The corresponding current density $\vec{J}_m$is given by

$$\vec{J}_m(\vec{r}, \vec{r}_q) = \frac{I}{4\pi} \frac{(\vec{r} - \vec{r}_q)}{|\vec{r} - \vec{r}_q|^3} \quad , \tag{5}$$

where σ is the specific conductivity of the material and I is the total current of the source. $\vec{r}$ is the observed point and the position of the source is $\vec{r}_q$. The field is radial symmetric.
In order to model the field of a tripole, three monopolar sources with different parameters (location, amplitude) are used and their fields are summed to receive the field of the according tripole:

$$\phi_t(\vec{r}, \vec{r}_{q1}, \vec{r}_{q2}, \vec{r}_{q3}, \vec{a}) = a_1\phi_m(\vec{r}, \vec{r}_{q1}) + a_2\phi_m(\vec{r}, \vec{r}_{q2}) + a_3\phi_m(\vec{r}, \vec{r}_{q3}) \tag{6}$$

and

$$\vec{J}_t(\vec{r}, \vec{r}_{q1}, \vec{r}_{q2}, \vec{r}_{q3}, \vec{a}) = a_1\vec{J}_m(\vec{r}, \vec{r}_{q1}) + a_2\vec{J}_m(\vec{r}, \vec{r}_{q2}) + a_3\vec{J}_m(\vec{r}, \vec{r}_{q3}) \quad , \tag{7}$$

where r_{qi} is the location and a_i the amplitude of pole i . In order to fulfill the necessity of closed current loops, the amplitudes a_i have to sum to one. In general, this could be added as a constraint but our results reveal that this is implicitly taken care off.

The tripolar model approaches tested within this paper were taken from three different sources:

- *Tripole A*: A negative sink with amplitude -300 nA was placed at -1 mm and a -120 nA charge 2.8 mm away from a central 420 nA source [Merletti and Farina, 2016].
- *Tripole B*: Two negative sinks (-210 nA) were set -1.6 mm and 3.2 mm away from a central double positive source (420 nA) [Roeleveld et al., 1997].
- Tripole C: two negative charges were set -2.1mm and 4.8mm from a central double positive source [Kuiken et al., 2001]

For source modeling, the source orientations are commonly oriented in the physiologically motivated direction, which is along the muscle fiber in EMG. In source reconstruction on the other hand, a regular grid is

spread over the scalp to avoid implicit geometric errors by the head models. This is a common approach also in neural source reconstruction in particular with generic head models.
In order to make common dipolar fitting routines work with the tripolar approach, we use the following approximation: Three tripoles are modeled around a central location in each direction of a Euclidean ACPC coordinate system. Their moments are determined during fitting in the same way as for a dipole. Secondly, the linear combination of the three tripoles, that minimizes the error, is determined..

Fig. 3 shows, that a tripole's scalp potential is not necessarily consisting of three patterns, even in proximity to the source. When using a tripole model with non-equal distance between the monopoles, in particular one of sources's surface patterns is weakened. The used muscular tripole models are actually very similar to dipoles except that the potential and current distributions are dominated by the stronger source-sink pair. A stronger source-sink pair can either be reached by a larger distance between the sources or by bigger source charges.

Building artefact models from MRI segmentation

For a realistic artefact source model, detailed muscle and eye positions within the head are essential. However, common MRI scans lack the necessary resolution and segmentation techniques to deduce the relevant anatomical details of muscles and eyes. Therefore, the open source Multimodal Imaging-Based Detailed Anatomical (MIDA) model of the human head and neck [Iacono et al., 2015], an open source, high-resolution MRI scan, segmented manually by experts, has been employed. The segmented tissue surface meshes were subject to post-processing, source model construction and warping to MNI space.

MIDA Open Source Atlas
MIDA has been obtained by segmenting high-resolution T1- and T2-weighted MRI scans, magnetic resonance angiography (MRA) and diffusion tensor imaging (DTI) data of one healthy 29-year old female volunteer. It was acquired at the Institute for Biomedical Engineering of the ETH Zurich (Switzerland) and contains 153 structures, segmented at 500 μm isotropic resolution.

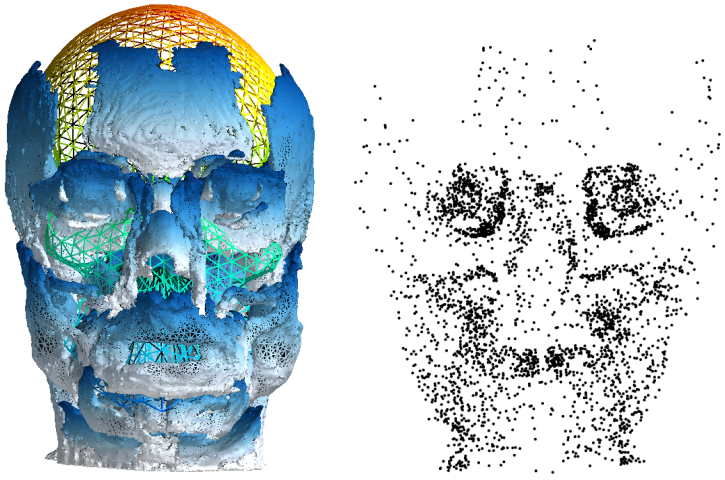

Figure 4: Face muscle positions and directions (left) [Schünke et al., 2007], muscular surface meshes mapped onto the skull mesh of the corresponding BEM head model (middle) and artefact source grid of size 3,5k (right).

Surface mesh corrections
The segmented face and neck muscle meshes as shown in the center of fig. 4 were corrected for self-intersections, unconnected nodes and duplicated elements. Unconnected mesh parts were detected and removed. The triangulated surfaces were simplified, coarsened to an appropriate number of mesh vertices and qualitatively enhanced (uniformity), while preserving the manifold.

Sourcemodel grid creation
Evenly spaced grids of 1 mm size were constructed within every muscle surface, building the artefact model's source positions. For the source reconstruction, however, regularly spaced grids were used as described above. According to the propagation direction of the MUAPs, the source's pole orientations should follow the muscle's fiber directions for simulation (see sec.). The fiber directions were approximated by using a Principial Component Analysis (PCA) on close neighboring grid points of a muscles grid point cloud, where the closeness criteria has been varied depending on the underlying muscle shape.
For eye activity, source grids were built for in total six tissues. Firstly, the retina of the left and right eye was modelled with orientations pointing in the positive y-axis of the ACPC coordinate system (i.e. forward). Secondly two source grids each were placed into the Cornea of the left and right eye, where one of them is oriented horizontally and the other vertically.

Warping to MNI coordinates
A warping procedure for transferring the artefact sourcemodel from MIDA into MNI space was developed, which interpolates every point within the scalp mesh of one person into the scalp mesh of another person.
It is noteworthy, that the MIDA scalp, skull and cortex surface meshes could not be segmented from MRI, since the original MRI scan was not publicly available.

Inverse Fitting Routines

We used three different inverse fitting routines: *dipfit_gridsearch* and *dipfit_nonlinear* based on fieldtrip's ft_dipolefitting [Oostendorp and Van Oosterom, 1989, Oostenveld et al., 2011] and *nonlinear_monopole* implementing a non-linear optimization for single monopolar positions. Location and orientation of the dipoles were adjusted in an iterative procedure in an attempt to maximize the amount of variance in the data explained by the model. One criterion for evaluation and comparison of models therefore was the 'relative residual variance' (RV), the relative amount of variance in the data, which is unexplained by the model [Scherg and Berg, 1991].
The RV is a sum-of-squares type error function, that focuses on relative deviations from the target pattern. The formula we employed is based on the scalp potentials measured (x) and estimated by the head model ($\hat{x}$):

$$RV = \frac{\sum (x - \hat{x})^2}{\sum x^2} \tag{8}$$

The RV has the advantage of being insensitive to the actual amplitude of the measured signal.
dipfit_gridsearch compares the RV of the potentials at the electrodes with the computed HArtMuT leadfields for every source point in the full sourcemodel (cortical + artefactual). The sources were placed at a regular grid within the scalp and brain. The source position combined with an orientation, that produced the lowest RV with the scalp pattern, then comprises the linear result to the inverse problem.
Subsequently, the nonlinear result for *dipfit_nonlinear* was achieved by allowing a minimization algorithm to vary orientation and source position using the *dipfit_gridsearch* results as starting points.
The tripolar moment of these fieldtrip based optimizations for tripoles was estimated in a similar fashion. It is the linear combination of three fields in each direction of Euclidean space using the fields of three monopoles each, as described in sec. .
For some of the results a further optimization routine, *nonlinear_monopole* was performed in order to see, if the source model was optimal. Single monopoles with individual amplitudes were therefore placed around the central position, that was found using *dipfit_nonlinear*. The positions and amplitudes were optimized for all

three monopoles at once, while iterating until convergence or the onset of a stopping criterion. A Levenberg-Marquardt [Moré, 1978] based non-linear optimization routine was employed and the error measure was again given by the RV.

Validation

HArtMuT's application to the inverse problem was validated against simulated EEG scalp patterns and subsequently on a real experimental EEG data set.

In the first validation step (simulated data), an FEM was used as 'ground-truth' head model to validate the model and the inverse fitting routines and the results were compared to those of a standard 3-shell BEM model from EEGLAB [Delorme and Makeig, 2004a]. Therefore, scalp patterns of dipolar sources were first simulated at all muscle positions from MIDA using the FEM and then the inverse fits were performed using a regular grid (resolution 10mm) within the head (only brain and scalp sources considered) as described above. The second (experimental data) validation was performed using data from an EEG experiment (see Gramann et al. [2021] for a description of the data). From the experimental data, different components and their scalp patterns were extracted using Independent Component Analysis (ICA; [Makeig et al., 1996b]) within EEGLAB [Delorme and Makeig, 2004b]. For each independent component (IC), the source point from a regular grid (resolution 10mm) within the head (only brain and scalp sources considered) was estimated based on the criterion that its BEM modeled scalp potential has the smallest distance to the scalp potential of the respective IC (measured in RV).

Simulated Data

NYhead

The simulated scalp patterns were calculated by use of the anatomy of the NYhead [Huang et al., 2016]. The NYhead is a high resolution Finite Element Model (FEM), that includes the neck. Its mesh and 75k cortical leadfields are publicly available. Since the published leadfields were calculated using the proprietary *Abaqus FEA software suite*, the cortical leadfields were recalculated using the open source software package SimBio. Comparing both the original Abaqus Software and the SimBio leadfields simulation, an average correlation of 0.66 for single source location leadfields was found. The discrepancy may be explained by the use of different solvers and an additional linear source point and electrode transformation, applied beforehand. The transformation was needed to bring FEM mesh and source and electrode positions into the same coordinate system.

Using the NYhead, leadfields of an 3,5k big artefact source model were calculated at the same 129 aligned electrodes from the dataset of the experimental data validation. Each leadfield was used as single scalp pattern, to which the corresponding source position was localized using HArtMuT and the inverse fitting routines described in sec. .

Results

The results of the source localization on simulated dipolar cortical and artefactual source points are plotted in fig. 5. The source localization error for brain and artefact sources using the HArtMuT 4-shell model was estimated to be around 10mm with an RV mainly around 0.01. This deviation from the simulated sources was to be expected for approximating a FEM with a BEM using different head geometries and thus also non perfectly matching electrode and source model positions in coarser grids (10mm) (compare Miklody et al. [2016]). It has to be pointed out, that the RVs are far below 0.1 (even the upper quartiles) and the resulting patterns were highly similar, which points towards a good fit but difference in geometry.
In comparison, the commonly used EEGLAB 3-shell model performed much worse for all sources. The median source localization error was above 20mm for the brain and close to 30mm for artefacts. This is of course also an effect of the head model missing the lower head region including the neck, where a lot of artefact sources lie, but is especially an effect of general model error for the brain sources.

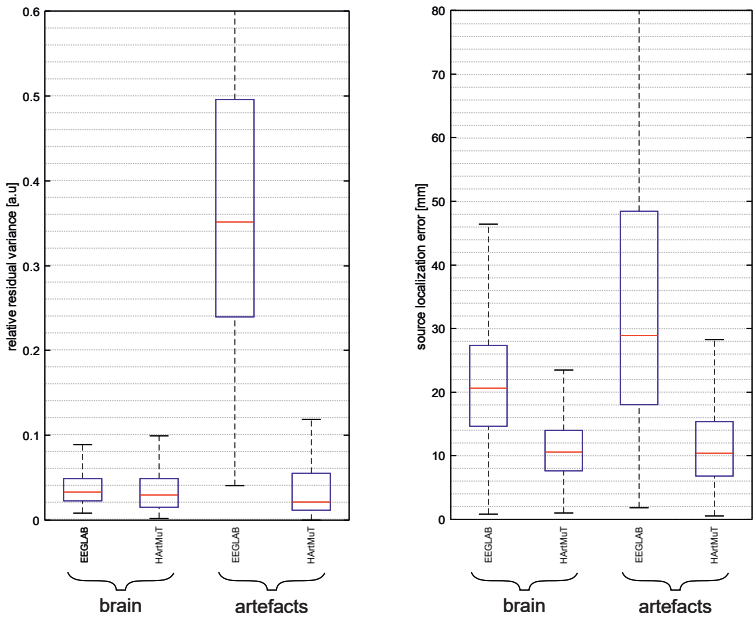

Figure 5: The relative residual variance (RV) and the geometrical error in source localization using *dipfit_gridsearch* for FEM-simulated scalp potentials reconstructed using the HArtMuT 4-shell BEM head model remained reasonably low (RV median 0.025 and source reconstruction error around 10mm)). The geometries of the two models (NYhead vs. Colin27) were not exactly the same, such that the electrode and source positions needed to be transformed, mimicking a realistic scenario. The standard 3-shell model lead to significantly higher RV for brain than for artefact sources than the 4-shell for all subjects. These findings are even stronger in the source reconstruction error.

Summary/Remarks

The performed validation against simulated data from a HD-FEM model was successful. This validates in particular HArtMuTs BEM model as a whole, the used inverse fitting routine, the neck extension procedure developed and applied to Colin27, and furthermore the translation procedure between the different head shapes (MIDA, NYhead, Colin27). Another result is, that the RV does not necessarily reflect the source localization error, which can be seen by looking at some of the 3-shell lower RVs of the brain being in a similar range as for the 4-shell while the source localization errors are all much higher.
Moreover, the artefact position warping routine introduced further uncertainty, since the MRI scan was based on a nonlinear warping routine of cortex positions.

Experimental data

In a second validation, ICA components extracted from real experimental EEG data were used as ground truth. We reconstructed and localized the source patterns using different models involving the commonly used 3-shell BEM dipole and a variety of dipolar and tripolar models based on a 4-shell BEM head model. First the different source models were used with the inverse fitting routines and the resulting relative residual variances (RVs) were then compared to see, which model best described the experimental data patterns, and thus, which model overall demonstrated the best fit for the different types of sources.

Data and processing

The data of 19 healthy subjects (11 female, 8 male, aged 20-46 years, M = 30.25 years) was recorded in another study [Gramann et al., 2021], focusing on heading computation in a stationary and a mobile experimental condition. The virtual environment consisted of a simple floor rendering without external

landmarks. Each trial started with a pole (indicating zero heading) which was then replaced by a sphere moving around the participant at a constant distance but with different velocity profiles. Participants were instructed to follow the movement of the sphere and to rotate back after the sphere stopped moving unpredictably at eccentricities between 30 and 150 degrees to the left or right. In the stationary condition, participants followed the sphere using a joystick while standing in front of a 2D monitor. In the mobile condition, they physically rotated wearing a virtual reality head-mounted display. Rotation eccentricity, speed, and direction were varied across 140 trials per movement condition (stationary vs. mobile). For the present study and modelling approaches, only the full-body rotation condition was taken into account, as we were interested in the contributions of neck muscles and eye movements to the sensor signal.
EEG data was recorded with 1 kHz sampling rate from 157 active electrodes (BrainProducts, Gilching, Germany) with 129 channels in a cap with equidistant layout (with two vertical EOG channels, both eyes) and 28 channels in a custom neckband. Individual electrode locations were recorded (Polaris Vicra, NDI, Waterloo, ON, Canada). Additional motion data was recorded but is not considered for the modelling approach in this study.
The data was processed in MATLAB (R2016b version 9.1; The MathWorks Inc., Natick, Massachusetts, USA) using custom scripts based on the EEGLAB toolbox [Delorme and Makeig, 2004a, version 14.1.0]. The 28 channels located in the neckband did not increase the decomposition quality of the ICA [Klug and Gramann, 2021] and were thus removed. Subsequently, the data was re-sampled to 250 Hz, line noise was removed with Zapline [de Cheveigné, 2020] using default settings, and breaks and pre-/post-experiment segments were removed from the data. We then used the "clean_rawdata" function of EEGLAB to detect and interpolate bad channels (disregarding EOG channels) using an 0.8 correlation threshold and no other measures. Subsequently the data was re-referenced to the average of all channels except the EOG channels. We then applied a 1 Hz high-pass filter as suggested by Klug and Gramann [2021] and computed an ICA using the AMICA algorithm [Palmer et al., 2011] with 2000 iterations and automatic rejection of samples (3 times with 3 SD threshold). Subsequently, for each independent component, an equivalent dipole model was computed using the dipfit routines from EEGLAB. Finally, components were labeled using the ICLabel "lite" classifier [Pion-Tonachini et al., 2019].

Results

The results are shown in fig. 6. Following ICA decomposition, the 19 subjects had on average 112 components depending on the number of valid channels after the preceding artefact channel rejection and rank of the data. Compared to using standard EEGLAB 3-shell models, the residual variance was reduced from median 0.25 to 0.11 for muscle sources and 0.18 to 0.09 for eye sources.
Of the total 2132 extracted components of all subjects, 68% were detected as muscle sources based on source location in the 4-shell HArtMuT, while 30% were brain and around 2% symmetric eye sources. The amplitudes of eye sources was overall strongest (median $8.8\mu V$, maximum $419.0\mu V$) followed by muscle sources (median $0.4\mu V$, maximum $181.1\mu V$) and brain sources (median $0.2\mu V$, maximum $36.0\mu V$).
Using the simple *dipfit_gridsearch*, tripoles reduced the RV compared to dipoles for 3/19 subjects ($\alpha \leq .05$). When we further optimized the source positions using *dipfit_nonlinear*, the difference in error between dipoles and tripoles were not siginificant any more except for one subject ($\alpha \leq .05$). Using *dipfit_nonlinear* significantly ($\alpha \leq .05$) reduced the errors within any source model in every subject.
For the eyes, using dipolar models symmetrically aligned around the x-axis (ACPC coordinate system) with equal amplitudes lead to the lowest error using *dipfit_gridsearch* compared to any other combination. *dipfit_non-linear* was not implemented in this case.

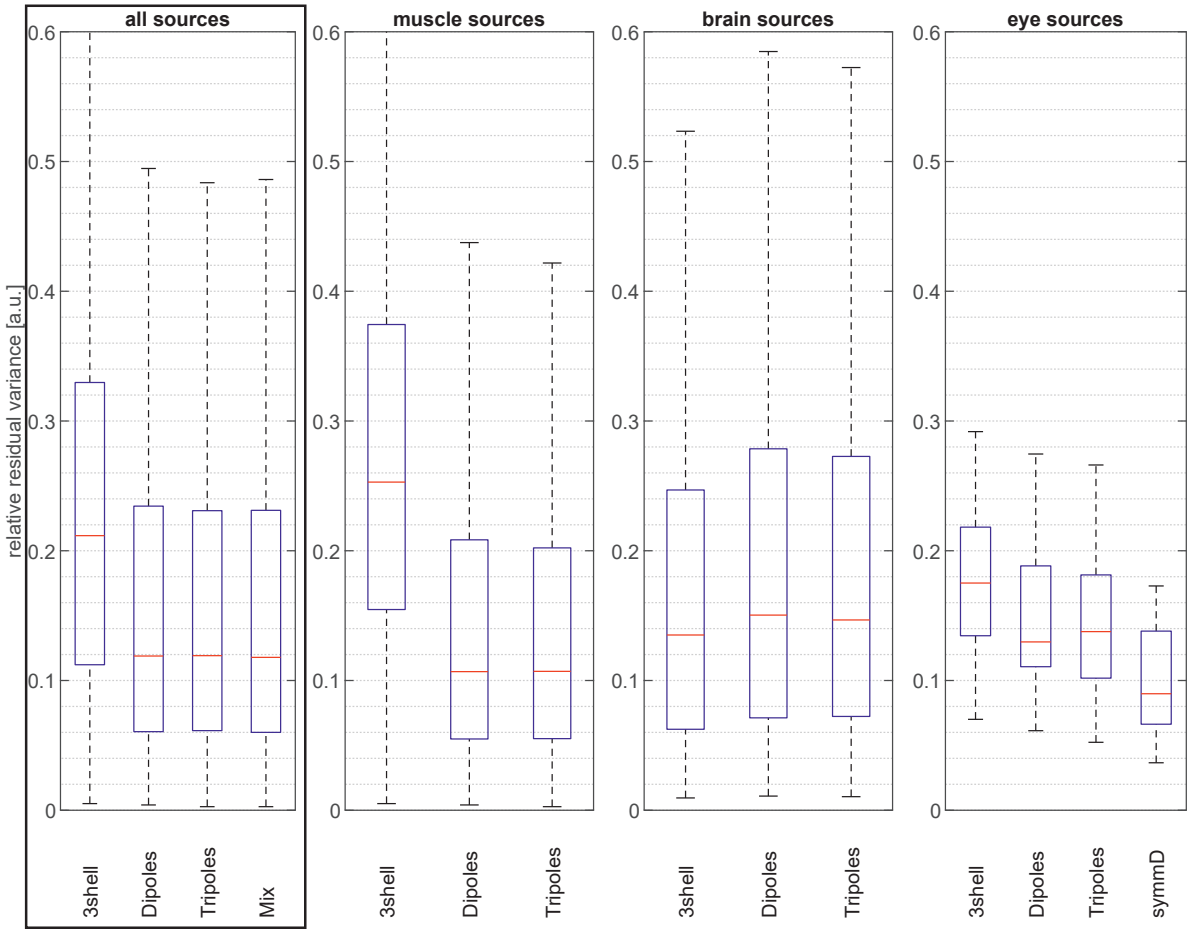

Figure 6: The residual variance of the source reconstruction results for different source models using *dipfit_nonlinear* over 19 subjects: Tripoles lead to significantly lower errors for muscles than dipoles in 2/19 subjects ($\alpha < 0.5$) while additionally 2 are touching significance ($\alpha = 0.5$). Symmetric dipoles (symmD) led to the lowest errors for eye sources. For cortical sources, dipoles led to significantly lower errors than tripoles while the traditional 3shell produces lowest errors. A mix of dipoles for the brain, tripoles for muscle and symmetric dipoles for eye sources lead to the lowest errors overall. The commonly used 3-shell model produced significantly the highest RVs in all subjects except for brain sources. Note, that the symmetric dipoles (symmD) were only fitted using *dipfit_gridsearch* and could be potentially improved by the nonlinear fit.

Comparing different approaches for modeling the muscles in fig.7, Tripole B lead to the lowest median and lower quartile errors, which is why it was also used as the main model of HArtMuT, altough the differences were not significant.

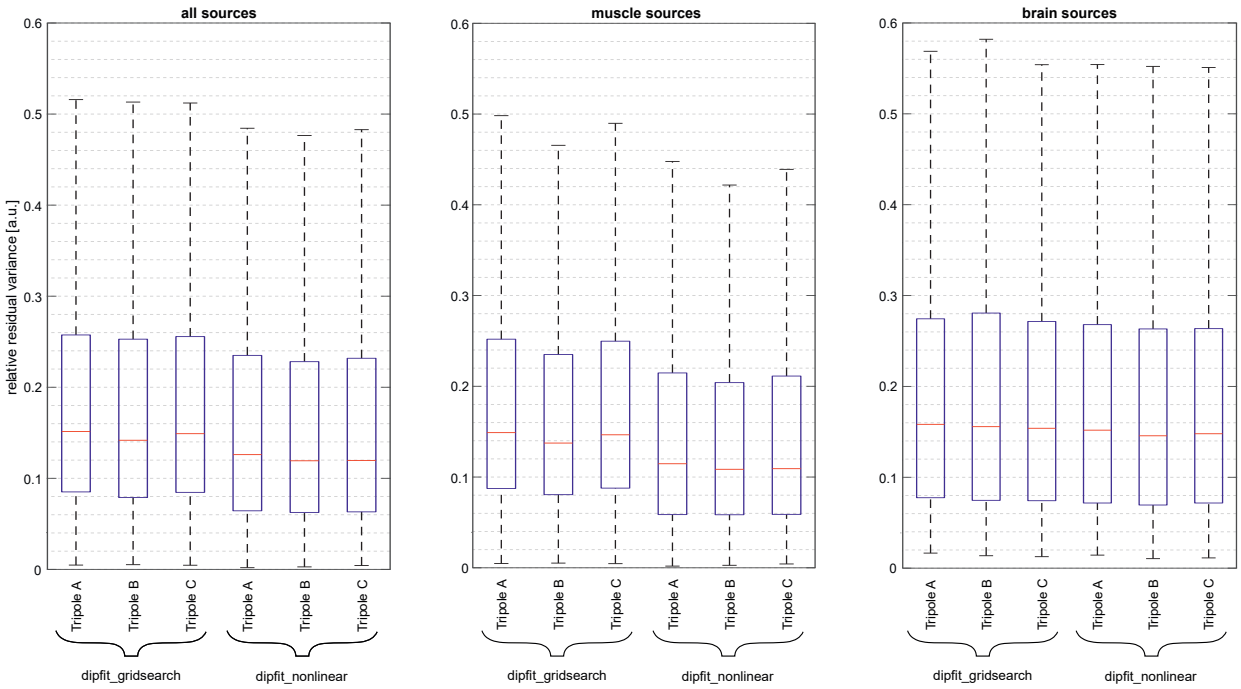

Figure 7: The residual variance of the source reconstruction results for different muscular models using different source localization algorithms: Tripole B leads to lowest, C to second lowest and Tripole A to highest errors. The differences were not significant.

Looking at the exemplary reconstructed patterns in figure 8 on the right, dipolar and tripolar patterns remained similar with comparable RV values. Compared to the original ICA patterns, the approach of using 3 monopoles leads to the best-matching (lowest RV) results. The magnified source locations and moments for the different models showed a general similarity in moments between the dipole and Tripole B, while the locations slightly differed. The 3 monopoles leading to the best results on average, were placed in proximity to the other solutions, while their individual positions and distances differed from that of the standard dipole. They were not arranged in one line and not uni-distant while the amplitudes additionally varied slightly.

Most of the muscular IC patterns were localized close to the Muscle temporalis or temporoparietalis (27.5%), followed by a MIDA's unspecific M. generalis class (20.6%), which is a collection of muscular tissue in the very bottom. Then it follows the M. splenius capitis (10.6%), M. occipitiofrontalis (9.6%) and M. trapezius (5.4%). All other muscles (27 in total) were below 4% in their occurrences.

We also investigated the resulting classification based on source location with automatic IC classification by dipfit using IClabel, an EEGLAB plugin, that automatically classifies IC components into different classes based on a classifier, which was built with a crowd labeling approach [Pion-Tonachini et al., 2019].

Correspondence between IC classification based on IClabel and localization in the mixed 4-shell HArtMuT source model with dipolar sources for the brain, tripolar for muscle and symmetric dipolar for brain:

		IClabel						
		brain	muscle	eye	heart	line noise	channel noise	other
HArtMuT	brain	12.9%	2.3%	0.1%	0.0%	0.8%	0.4%	13.6%
	muscle	2.7%	39.6%	1.7%	0.3%	0.6%	6.8%	16.0%
	eye	0.0%	0.5%	1.2%	0.0%	0.0%	0.0%	0.4%

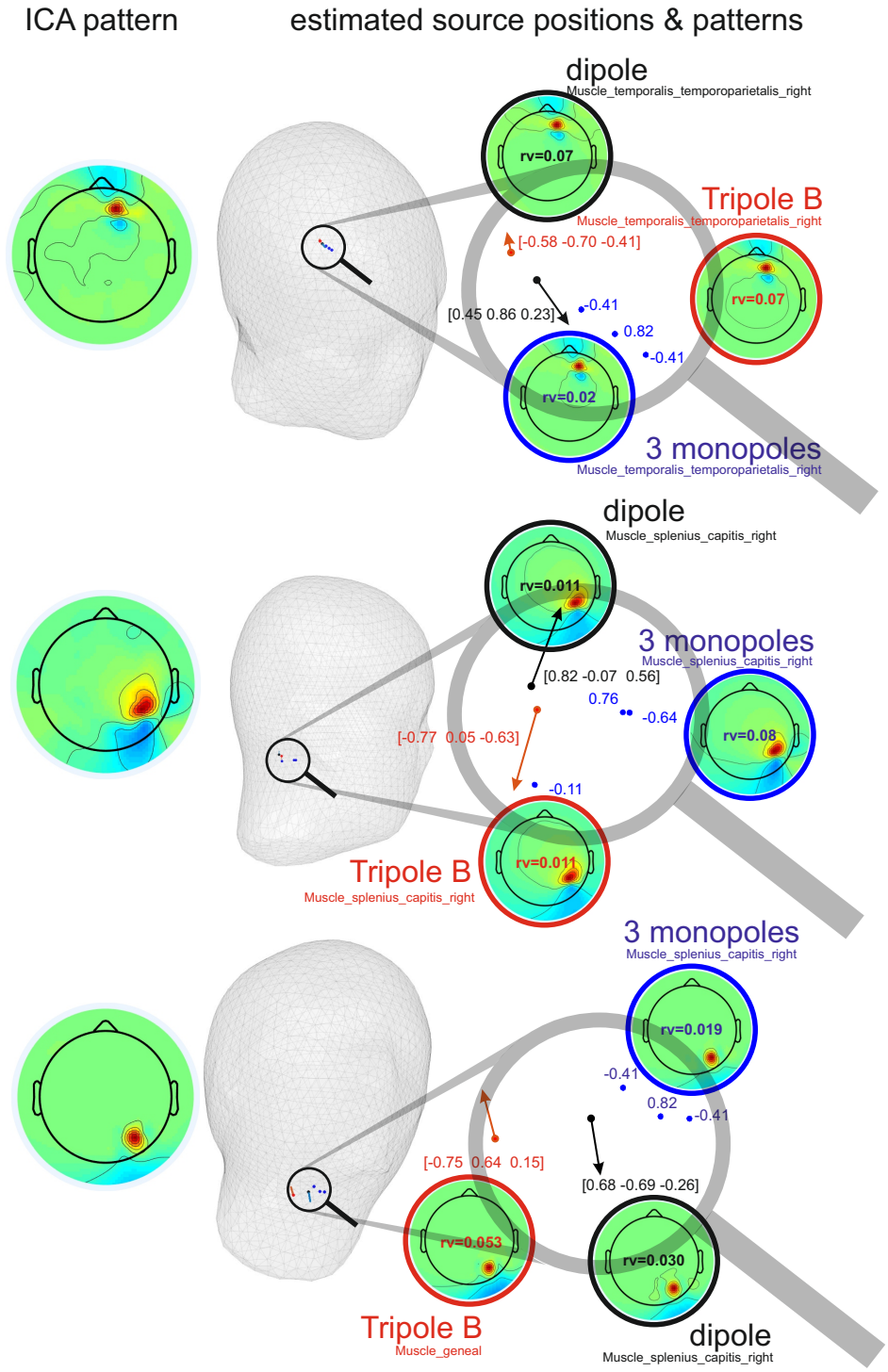

Figure 8: Three exemplary source models and their solution in source localization for muscle artefacts: on the left you can find the independent component extracted from the data, in the center is the location in the head while on the right you find a detailed relative positioning of the three models and their corresponding patterns. Black is the dipolar model and moment, red tripolar with Tripole B and blue after non-linear optimization of three monopoles. Here, the numbers represent the amplitude of each monopole.

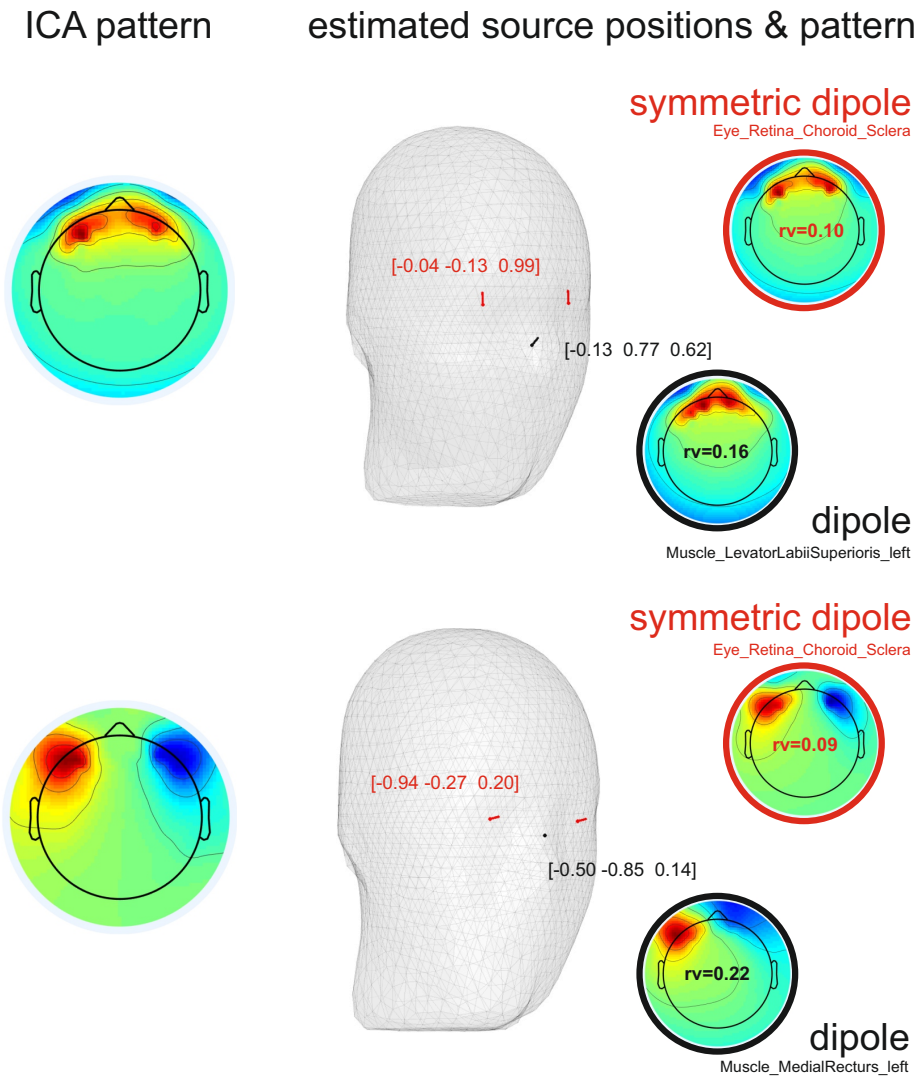

Figure 9: Two exemplary source models and their solution in source localization for eye artefacts. On the left you can find the independent component extracted from the data, in the center is the fitted location in the head while on the right you find a detailed relative positioning of the two models and their corresponding patterns. Black is the dipolar model and moment and red the symmetric dipole.

This simple approach, in which only the comparison of the scalp patterns of the forward model with IC patterns is incorporated, already leads to a high correspondence between the IC classification labels and the resulting source location based classification. Of the ICs classified as brain by IClabel, there were 83% equally classified as brain by HArtMuT and for the muscles 93% as muscles. The median RV of IC classification as "other" was 0.22 opposing all remaining classes 0.096. The components classified as 'eye' by IClabel are 57% classified as muscles and 40% as eyes using symmetric dipoles. It is of course not assured, that IClabel classified correctly but this large correspondence is notable.

In figure 9 the clear difference between symmetric and non-symmetric dipolar eye models can be investigated. As we expected, the best eye models concerning the pattern reconstruction error are linked symmetrically. Here, the simple *dipfit_gridsearch* outperforms all other models, that use non-symmetric tripoles and dipoles.

In the source locations we see, that for these models, the source was mostly located somewhere between the eyes, which is not realistic.

Most ocular sources were found to lie in or close to the Retina (84%), while the rest lie in or close to the Cornea (16%). Interestingly, the commonly found pattern on the bottom in 9 corresponds to the straight forward looking eye position. The approach only catches static eye positions in single independent components and eye movements will be spread over linear combinations of static patterns such as the upper for upwards movements away from the lower straight forward position. A *dipfit_nonlinear* routine for linked symmetric positions had not been implemented within this work, but is expected to further improve the results.

Discussion

We investigated new approaches of modeling muscle and eye contributions to EEG and used the models in a source reconstruction on simulated and experimental data.
In sum, we propose our new head model HArtMuT, which includes the neck and corresponding brain, muscle and eye tissue source positions and labels. It is avialable for different head anatomies and BEM/FEM models. We tested the effect of modelling sources as dipoles, tripoles, three monopoles, and symmetric dipoles and measured the performance on simulated and experimental data in residual variance and localization error. The best option is a combination of the three models depending on the tissue type, while a dipolar model is sufficient for most use cases. This best combination consists of dipoles for the brain, tripoles for the muscles and symmetric dipoles for the eyes.
Compared with the standard EEGLAB 3-shell BEM, our proposed head model appears to be a general improvement. We showed that the localization error and RV values using simulated ground truth data (based on an FEM head model) were lowest with our new head model. We also validated the model on real experimental EEG data of moving subjects and found that RV values of our model were lower, especially considering muscle and eye sources. The latter were about the same level as the brain sources in our model, which is not the case in the standard model. A comparison with IClabel indicates, that HArtMuT may be a promising tool not only for source localization but also for classification of ICs.

In a validation of the method on simulated and experimental data, it was found that our headmodel improved over the commonly used EEGLAB 3-shell model in particular for muscle and eye sources. Furthermore, muscle and eye artefacts could clearly be differentiated from brain sources by their patterns using inverse fitting routines together with an appropriate model.

While a single dipole model is most likely sufficient for a reasonably good source localization of all components except the eyes, a tripolar model is appropriate for muscle sources and a symmetric dipolar model for the eyes. A tripolar model for muscular sources, which is commonly used in EMG recordings of other body parts and is justified by the triphasic muscular action potential, did improve the estimation of source potentials for muscles for some of the subjects and interestingly also for the brain. For the eyes, a symmetric dipolar model led to the lowest approximation errors as was expected from the synchronous movements of the eyes.

The fact, that three single monopoles placed through non-linear optimization, were the best approximations to exemplary muscle sources has two consequences: first, the field of muscles does not have a clear unifying model such as commonly assumed in the dipole of the brain sources, and second, the local field is more important for muscles. A far-field approximation such as the dipole is reasonable in a first approximation as the tripolar muscle source is close to a dipole on first approximation. For a better model it is probably necessary to use three single monopoles with individual parameters as the distances between sources and sensors is much smaller for sources in the scalp and both are in the same tissue. The scalp is a mixture of tissues with approximately similarly conductive properties leading to less spatial smearing. The signals from the brain in contrast still have to propagate through the more conductive CSF and the low-conductive skull, which strongly distorts the signals.

As we can additionally draw from the internal validation using a BEM to approximate an FEM head model, we find, that localization errors can easily be much larger as systematic differences in geometries, source and

sensor locations contribute to the error.

For a very good approximation of muscular scalp potentials it seems essential to know the individual geometry and to use the best possible head model with an appropriate source model. The present study indicates that this would be a FEM head model with a distributed source model. However, a reasonable approximation to this combination would be a model of single monopoles. If this is not at hand, a dipolar model, which is commonly implemented in simulations suits, is sufficient for source localization and muscle identification. It can also be used to differentiate brain from muscle sources as the differences are already visible in the patterns of dipoles. This is also supported by the correspondence with the IClabel classification based labels.

It remains an open question whether the case of *dipfit_nonlinear* optimized 3-shell RV of brain ICs being significantly below the other for all subjects means that our model is not optimal here, or that the 3-shell just produces lower RVs. In general, the RV only tells about fitting quality from a numeric perspective, not plausibility. Also, the 3-shell model was only built down to the level of the nose. All electrodes below are projected onto this surface. It might just be possible to reach lower RVs because of this model error. Another factor might be non-optimal tissue conductivities in the 4-shell headmodel. A post-hoc analysis reveled that HArtMuTs RVs can be improved for the brain to a similar level by matching conductivities. Another reason could be missing anatomical correspondence for the high detailed model because a generic anatomy was used. It could be that the 3-shell is delivering lower errors because it is more generic with its constant skull thickness. We will investigate this further in another study.

Concerning the use of the source localization results of the IC patterns in a classifier, HArtMuT delivers very promising results: the correspondence with EEGLAB IClabels is high and clear. However, the EEGLAB IClabel classifications are highly debated as the classifier was trained on EEG data from stationary participants only and can thus not be seen as the 'ground truth' in all studies. In this study, they were introduced to serve a basic intuition for the quality of results. A further study to investigate the usage of HArtMuT for artefact labels in detail is planned.

Aknowledgements

We want to thank Benjamin Blankertz for his outstanding general and logistical support of this project. NH acknowledges support from the Research Training Group (RTG 2433) DAEDALUS (Differential Equation- and Data-driven Models in Life Sciences and Fluid Dynamics) funded by Deutsche Forschungsgemeinschaft (DFG).

Contributions

Nils and Daniel implemented the segmentation and warping routines. Daniel took care of the BEM head models including tripolar model implementation. Nils implemented all FEM head models and the artefact atlas. Marius implemented the first versions of the dipfit routines in EEGLAB, which were then further improved Klaus had the original idea and was closely supporting the project in the beginning and in the final manuscript phase.

References

Stefan Haufe, Frank Meinecke, Kai Gorgen, Sven Dahne, John-Dylan Haynes, Benjamin Blankertz, and Felix Biessmann. Parameter interpretation, regularization and source localization in multivariate linear models. In *Pattern Recognition in Neuroimaging, 2014 International Workshop on*, pages 1–4. IEEE, 2014.

Karl Pearson. LIII. on lines and planes of closest fit to systems of points in space. *Philosophical Magazine Series 6*, 2(11):559–572, 1901. doi: 10.1080/14786440109462720.

Scott Makeig, Anthony J Bell, Tzyy-Ping Jung, and Terrence J Sejnowski. Independent component analysis

of electroencephalographic data. In *Advances in neural information processing systems*, pages 145–151, 1996a.

Benjamin Blankertz, Steven Lemm, Matthias Sebastian Treder, Stefan Haufe, and Klaus-Robert Müller. Single-trial analysis and classification of ERP components – a tutorial. *NeuroImage*, 56:814–825, 2011. URL http://dx.doi.org/10.1016/j.neuroimage.2010.06.048.

J Sarvas. Basic mathematical and electromagnetic concepts of the biomagnetic inverse problem. *Phys. Med. Biol.*, 32:11–22, 1987.

Jose Urigüen and Begoña Zapirain. Eeg artifact removal – state-of-the-art and guidelines. *Journal of neural engineering*, 12:031001, 04 2015. doi: 10.1088/1741-2560/12/3/031001.

Irene Winkler, Stefan Haufe, and Michael Tangermann. Automatic classification of artifactual ICA-components for artifact removal in EEG signals. *Behavioral and Brain Functions*, 7(1):30, 2011. ISSN 1744-9081. doi: 10.1186/1744-9081-7-30. URL http://www.behavioralandbrainfunctions.com/content/7/1/30.

Luca Pion-Tonachini, Ken Kreutz-Delgado, and Scott Makeig. Iclabel: An automated electroencephalographic independent component classifier, dataset, and website. *NeuroImage*, 198:181–197, 2019.

Laurens R. Krol, Juliane Pawlitzki, Fabien Lotte, Klaus Gramann, and Thorsten O. Zander. Sereega: Simulating event-related eeg activity. *Journal of Neuroscience Methods*, 309:13–24, 2018. ISSN 0165-0270. doi: https://doi.org/10.1016/j.jneumeth.2018.08.001. URL https://www.sciencedirect.com/science/article/pii/S0165027018302395.

A Gramfort, T Papadopoulo, E Olivi, and M Clerc. OpenMEEG: opensource software for quasistatic bioelectromagnetics,. *BioMedical Engineering OnLine*, 45:9, 2010.

Colin J Holmes, Rick Hoge, Louis Collins, Roger Woods, Arthur W Toga, and Alan C Evans. Enhancement of mr images using registration for signal averaging. *Journal of computer assisted tomography*, 22(2): 324–333, 1998.

Daniel Miklody, Yu Huang, Stefan Haufe, and Lucas Parra. Automatic creation of fast, realistic boundary element head models. In *2016 22nd Annual Meeting of the Organization for Human Brain Mapping (OHBM)*, 2016.

Daniel Miklody. *The neurophysiology of EEG and the physics of the head : theory and Application for Spontaneous EEG*. Doctoral thesis, Technische Universität Berlin, Berlin, 2020. URL http://dx.doi.org/10.14279/depositonce-10419.

M Häamäläinen, R Hari, RJ Ilmoniemi, J Knuutila, and OV Lounasmaa. Magnetoencephalography — theory, instrumentation, and applications to noninvasive studies of the working human brain. *Rev. Mod. Phys.*, 65:413–497, Apr 1993. doi: 10.1103/RevModPhys.65.413. URL http://link.aps.org/doi/10.1103/RevModPhys.65.413.

György Buzsáki, Costas A. Anastassiou, and Christof Koch. The origin of extracellular fields and currents - EEG, ECoG, LFP and spikes. *Nature Reviews Neuroscience*, 13:407–420, 2012. ISSN 1471-0048. doi: https://doi.org/10.1038/nrn3241.

Shingo Murakami and Yoshio Okada. Contributions of principal neocortical neurons to magnetoencephalography and electroencephalography signals. *The Journal of Physiology*, 575(3):925–936, 2006. doi: https://doi.org/10.1113/jphysiol.2006.105379. URL https://physoc.onlinelibrary.wiley.com/doi/abs/10.1113/jphysiol.2006.105379.

Masaki Iwasaki, Christoph Kellinghaus, Andreas V. Alexopoulos, Richard C. Burgess, Arun N. Kumar, Yanning H. Han, Hans O. Lüders, and R. John Leigh. Effects of eyelid closure, blinks, and eye movements on the electroencephalogram. *Clinical Neurophysiology*, 116(4):878 – 885, 2005. ISSN 1388-2457. doi:

https://doi.org/10.1016/j.clinph.2004.11.001. URL http://www.sciencedirect.com/science/article/pii/S138824570400416X.

Michael Plöchl, José Pablo Ossandón, and Peter König. Combining EEG and eye tracking: identification, characterization, and correction of eye movement artifacts in electroencephalographic data. *Frontiers in human neuroscience*, 6:278, 2012.

Patrick Berg and Michael Scherg. Dipole models of eye movements and blinks. *Electroencephalography and Clinical Neurophysiology*, 79(1):36 – 44, 1991. ISSN 0013-4694. doi: https://doi.org/10.1016/0013-4694(91)90154-V. URL http://www.sciencedirect.com/science/article/pii/001346949190154V.

D. Colin Boyd, Peter D. Lawrence, and Paul J. A. Bratty. On modeling the single motor unit action potential. *IEEE Transactions on Biomedical Engineering*, BME-25:236–243, 1978.

D.A. Winter, A.J. Fuglevand, and S.E. Archer. Crosstalk in surface electromyography: Theoretical and practical estimates. *Journal of Electromyography and Kinesiology*, 4(1):15 – 26, 1994. ISSN 1050-6411. doi: https://doi.org/10.1016/1050-6411(94)90023-X. URL http://www.sciencedirect.com/science/article/pii/105064119490023X.

Dario Farina and Alberto Rainoldi. Compensation of the effect of sub-cutaneous tissue layers on surface emg: A simulation study. *Medical engineering & physics*, 21:487–97, 07 1999. doi: 10.1016/S1350-4533(99)00075-2.

P.A.M. Griep, F.L.H. Gielen, H.B.K. Boom, K.L. Boon, L.L.W. Hoogstraten, C.W. Pool, and W. Wallinga-De Jonge. Calculation and registration of the same motor unit action potential. *Electroencephalography and Clinical Neurophysiology*, 53(4):388 – 404, 1982. ISSN 0013-4694. doi: https://doi.org/10.1016/0013-4694(82)90004-9. URL http://www.sciencedirect.com/science/article/pii/0013469482900049.

Roberto Merletti, Loredana Lo Conte, Elena Avignone, and Piero Guglielminotti. Modeling of surface myoelectric signals - part i: Model implementation. *IEEE transactions on bio-medical engineering*, 46: 810–20, 08 1999. doi: 10.1109/10.771190.

K Roeleveld, J.H Blok, D.F Stegeman, and A van Oosterom. Volume conduction models for surface emg; confrontation with measurements. *Journal of Electromyography and Kinesiology*, 7(4):221 – 232, 1997. ISSN 1050-6411. doi: https://doi.org/10.1016/S1050-6411(97)00009-6. URL http://www.sciencedirect.com/science/article/pii/S1050641197000096.

R. Merletti and D. Farina. *Surface Electromyography: Physiology, Engineering, and Applications*. IEEE Press Series on Biomedical Engineering. Wiley, 2016. ISBN 9781119082903. URL https://books.google.de/books?id=6kTfCwAAQBAJ.

P Rosenfalck. Intra- and extracellular potential fields of active nerve and muscle fibres. a physico-mathematical analysis of different models. *Acta physiologica Scandinavica. Supplementum*, 321:1–168, 1969.

S. D. Nandedkar and E. Stålberg. Simulation of single muscle fibre action potentials. *Medical and Biological Engineering and Computing*, 21(2):158–165, Mar 1983. ISSN 1741-0444. doi: 10.1007/BF02441531. URL https://doi.org/10.1007/BF02441531.

S Goncalves, JC de Munck, JPA Verbunt, Fetsje Bijma, RM Heethaar, and FH Lopes da Silva. In vivo measurement of the brain and skull resistivities using an EIT-based method and realistic models for the head. *IEEE Trans. Biomed. Eng.*, 50:754–767, 2003.

M Clerc, G Adde, J Kybic, T Papadopoulo, and JM Badier. In vivo conductivity estimation with symmetric boundary elements. *IJBEM*, 7:307–310, 2005.

T. A. Kuiken, N. S. Stoykov, M. Popovic, M. Lowery, and A. Taflove. Finite element modeling of electro-

magnetic signal propagation in a phantom arm. *IEEE Transactions on Neural Systems and Rehabilitation Engineering*, 9(4):346–354, Dec 2001. ISSN 1534-4320. doi: 10.1109/7333.1000114.

Maria Ida Iacono, Esra Neufeld, Esther Akinnagbe, Kelsey Bower, Johanna Wolf, Ioannis Vogiatzis Oikonomidis, Deepika Sharma, Bryn Lloyd, Bertram J Wilm, Michael Wyss, Klaas P Pruessmann, Andras Jakab, Nikos Makris, Ethan D Cohen, Niels Kuster, Wolfgang Kainz, and Leonardo M Angelone. Mida: A multimodal imaging-based detailed anatomical model of the human head and neck. *PloS one*, 10(4): e0124126–e0124126, 04 2015. doi: 10.1371/journal.pone.0124126. URL https://www.ncbi.nlm.nih.gov/pubmed/25901747.

M. Schünke, L.M. Ross, E. Schulte, E.D. Lamperti, and U. Schumacher. *Thieme Atlas of Anatomy: General Anatomy and Musculoskeletal System*. THIEME Atlas of Anatomy. Thieme, 2007. ISBN 9783131421012.

Thom F Oostendorp and Adriaan Van Oosterom. Source parameter estimation in inhomogeneous volume conductors of arbitrary shape. *IEEE transactions on biomedical engineering*, 36(3):382–391, 1989.

R Oostenveld, P Fries, E Maris, and JM Schoffelen. Fieldtrip: Open source software for advanced analysis of MEG, EEG, and invasive electrophysiological data,. *Computational Intelligence and Neuroscience*, 2011: Article ID 156869, 2011.

Michael Scherg and Patrick Berg. Use of prior knowledge in brain electromagnetic source analysis. *Brain topography*, 4(2):143–150, 1991.

JJ Moré. The levenberg-marquardt algorithm: Implementation and theory. In G.A. Watson, editor, *Numerical Analysis*, volume 630 of *Lecture Notes in Mathematics*, pages 105–116. Springer Berlin Heidelberg, 1978. ISBN 978-3-540-08538-6. doi: 10.1007/BFb0067700.

Arnaud Delorme and Scott Makeig. EEGLAB: An open source toolbox for analysis of single-trial EEG dynamics including independent component analysis. *Journal of Neuroscience Methods*, 134(1):9–21, 2004a. ISSN 01650270. doi: 10.1016/j.jneumeth.2003.10.009.

Klaus Gramann, Friederike U. Hohlefeld, Lukas Gehrke, and Marius Klug. Human cortical dynamics during full-body heading changes. *Scientific Reports*, 11(1):18186, 2021. ISSN 2045-2322. doi: 10.1038/s41598-021-97749-8. URL https://doi.org/10.1038/s41598-021-97749-8.

Scott Makeig, Anthony J Bell, Tzyy-Ping Jung, and Terrence J Sejnowski. Independent component analysis of electroencephalographic data. In *Advances in Neural Information Processing Systems 8: Proceedings of the 1995 Conference*, volume 8, page 145. MIT press, 1996b.

Arnaud Delorme and Scott Makeig. Eeglab: an open source toolbox for analysis of single-trial eeg dynamics including independent component analysis. *Journal of neuroscience methods*, 134(1):9—21, March 2004b. ISSN 0165-0270. doi: 10.1016/j.jneumeth.2003.10.009. URL https://doi.org/10.1016/j.jneumeth.2003.10.009.

Yu Huang, Lucas C. Parra, and Stefan Haufe. The new york head—a precise standardized volume conductor model for eeg source localization and tes targeting. *NeuroImage*, 140:150 – 162, 2016. ISSN 1053-8119. doi: https://doi.org/10.1016/j.neuroimage.2015.12.019. URL http://www.sciencedirect.com/science/article/pii/S1053811915011325. Transcranial electric stimulation (tES) and Neuroimaging.

Marius Klug and Klaus Gramann. Identifying key factors for improving ICA-based decomposition of EEG data in mobile and stationary experiments. *European Journal of Neuroscience*, 54(12):8406–8420, 2021. ISSN 0953-816X. doi: 10.1111/ejn.14992.

Alain de Cheveigné. ZapLine: a simple and effective method to remove power line artifacts. *NeuroImage*, 1 (1):1–13, 2020. ISSN 00127086. doi: http://dx.doi.org/10.1101/782029.

Jason A Palmer, Ken Kreutz-delgado, and Scott Makeig. AMICA : An Adaptive Mixture of Independent

Component Analyzers with Shared Components. *Swartz Center for Computatonal Neursoscience, University of California San Diego, Tech. Rep*, pages 1–15, 2011.